J|A|C|S ARTICLES

Published on Web 09/28/2009

Efficient Functionalization of Carbon Nanotubes with Porphyrin Dendrons via Click Chemistry

Thomas Palacin,[†] Hung Le Khanh,[†] Bruno Jousselme,[‡] Pascale Jegou,[‡] Arianna Filoramo,[†] Christian Ehli,[§] Dirk M. Guldi,*[,§] and Stéphane Campidelli*[,†]

CEA, IRAMIS, Laboratoire d'Electronique Moléculaire, SPEC, 91191 Gif sur Yvette, France, CEA, IRAMIS, Laboratoire de Chimie des Surfaces et Interfaces, SPCSI, 91191 Gif sur Yvette, France, and Department of Chemistry and Pharmacy and Interdisciplinary Center for Molecular Materials (ICMM) Friedrich-Alexander-Universität Erlangen-Nürnberg, Egerlandstrasse 3, 91058 Erlangen, Germany

Received July 20, 2009; E-mail: stephane.campidelli@cea.fr

Abstract: The attempt to decorate carbon nanotubes with organic molecules as a powerful means to form new functional materials has attracted broad attention in the scientific community. Here, we report the functionalization of single-walled carbon nanotubes (SWNTs) with zinc porphyrins (ZnP) using very mild conditions to afford a series of SWNTs−ZnP (**1** and **2**) electron donor−acceptor conjugates. Owing to the presence of either one or two ZnP, introduced via "click chemistry", different absorption cross sections were realized. Important in this context is that the covalent linkages between SWNT and ZnP were corroborated by monitoring the diagnostic signature of the nitrogen atoms as part of the formed triazole ring by X-ray photoelectron spectroscopy (XPS). The resulting SWNTs−ZnP **1** and **2** were fully characterized. This characterization was complemented by a full-fledged investigation of their electrochemical and photophysical properties. In particular, appreciably strong electronic coupling between the photo- and electroactive constituents (i.e., SWNT and ZnP) led to rapid excited-state deactivation of ZnP via charge transfer to the nanotubes. Here, the different absorption cross sections throughout the visible part of the solar spectrum turned out to be valuable in enhancing the overall light-harvesting features. Upon photoexcitation, for both SWNTs−ZnP **1** and **2**, radical ion pair states (i.e., reduced SWNT and oxidized ZnP) are formed. The charge-separated states decay to regenerate the singlet ground state with lifetimes of 820 and 200 ps for **1** and **2**, respectively.

Introduction

Carbon nanotubes possess exceptional electronic, mechanical, chemical, and optical properties, which render them particularly promising materials in the areas of solar energy conversion,[1−10] electronic, and sensing[11−19] as well as biological applications.[20−26]

Within the context of solar energy conversion and/or electronic applications, the control over associating single-walled carbon nanotubes (SWNTs) with photo- and electroactive building blocks constitutes a substantial challenge. Photoinduced processes between SWNTs and (i) electron donors, (ii) electron acceptors, or (iii) photoisomerizable molecules are important features for the fabrication of innovative optoelectronic devices

[†] CEA, IRAMIS, Laboratoire d'Electronique Moléculaire.
[‡] CEA, IRAMIS, Laboratoire de Chimie des Surfaces et Interfaces.
[§] Center for Molecular Materials (ICMM) Friedrich-Alexander-Universität Erlangen-Nürnberg.

(1) Guldi, D. M.; Rahman, G. M. A.; Zerbetto, F.; Prato, M. *Acc. Chem. Res.* **2005**, *38*, 871.
(2) Sgobba, V.; Guldi, D. M. *Chem. Soc. Rev.* **2009**, *38*, 165.
(3) Umeyama, T.; Imahori, H. *Energy Environ. Sci.* **2008**, *1*, 120.
(4) Imahori, H.; Umeyama, T. *J. Phys. Chem. C* **2009**, *113*, 9029.
(5) Rahman, G. M. A.; Guldi, D. M.; Cagnoli, R.; Mucci, A.; Schenetti, L.; Vaccari, L.; Prato, M. *J. Am. Chem. Soc.* **2005**, *127*, 10051.
(6) Guldi, D. M.; Rahman, G. M. A.; Sgobba, V.; Kotov, N. A.; Bonifazi, D.; Prato, M. *J. Am. Chem. Soc.* **2006**, *128*, 2315.
(7) Landi, B. J.; Castro, S. L.; Ruf, H. J.; Evans, C. M.; Bailey, S. G.; Raffaelle, R. P. *Sol. Energy Mater. Sol. Cells* **2005**, *87*, 733.
(8) Raffaelle, R. P.; Landi, B. J.; Harris, J. D.; Bailey, S. G.; Hepp, A. F. *Mater. Sci. Eng., B* **2005**, *116*, 233.
(9) Bhattacharyya, S.; Kymakis, E.; Amaratunga, G. A. J. *Chem. Mater.* **2004**, *16*, 4819.
(10) Ago, H.; Petritsch, K.; Shaffer, M. S. P.; Windle, A. H.; Friend, R. H. *Adv. Mater.* **1999**, *11*, 1281.
(11) Freitag M. Carbon nanotube electronics and devices. In *Carbon Nanotubes: Properties and Applicatons*; O'Connell, M. J., Ed.; CRC Press: Boca Raton, FL, 2006; pp 83−117.
(12) Avouris, P.; Chen, Z.; Perebeinos, V. *Nat. Nanotechnol.* **2007**, *2*, 605.
(13) Avouris, P.; Freitag, M.; Perebeinos, V. *Nat. Photonics* **2008**, *2*, 341.
(14) Kauffman, D. R.; Star, A. *Small* **2007**, *3*, 1324.
(15) Grüner, G. *J. Mater. Chem.* **2006**, *16*, 3533.
(16) Cao, Q.; Rogers, J. A. *Adv. Mater.* **2009**, *21*, 29.
(17) Snow, E. S.; Perkins, F. K.; Robinson, J. A. *Chem. Soc. Rev.* **2006**, *35*, 790.
(18) Grüner, G. *Anal. Bioanal. Chem.* **2006**, *384*, 322.
(19) Balasubramanian, K.; Burghard, M. *Anal. Bioanal. Chem.* **2006**, *385*, 452.
(20) Katz, E.; Willner, I. *ChemPhysChem* **2004**, *5*, 1084.
(21) Yang, W.; Thodarson, P.; Gooding, J. J.; Ringer, S. P.; Braet, F. *Nanotechnology* **2007**, *18*, 412001.
(22) Lin, Y.; Tailor, S.; Li, H.; Shiral Fernando, K. A.; Qu, L.; Wang, W.; Gu, L.; Zhou, B.; Sun, Y.-P. *J. Mater. Chem.* **2004**, *14*, 527.
(23) Bianco, A.; Kostaleros, K.; Partidos, C. D.; Prato, M. *Chem. Commun.* **2005**, 571.
(24) Kostaleros, K.; Lacerda, L.; Pastorin, G.; Wu, W.; Wieckowski, S.; Luangsivilay, J.; Godefroy, S.; Pantarotto, D.; Briand, J.-P.; Muller, S.; Prato, M.; Bianco, A. *Nat. Nanotechnol.* **2007**, *2*, 108.
(25) Kam, N. W. S.; O'Connell, M.; Wisdom, J. A.; Dai, H. *Proc. Natl. Acad. Sci. U.S.A.* **2005**, *102*, 11600.
(26) Kam, N. W. S.; Dai, H. *J. Am. Chem. Soc.* **2005**, *127*, 6021.

 10.1021/ja906020e CCC: $40.75

Chart 1

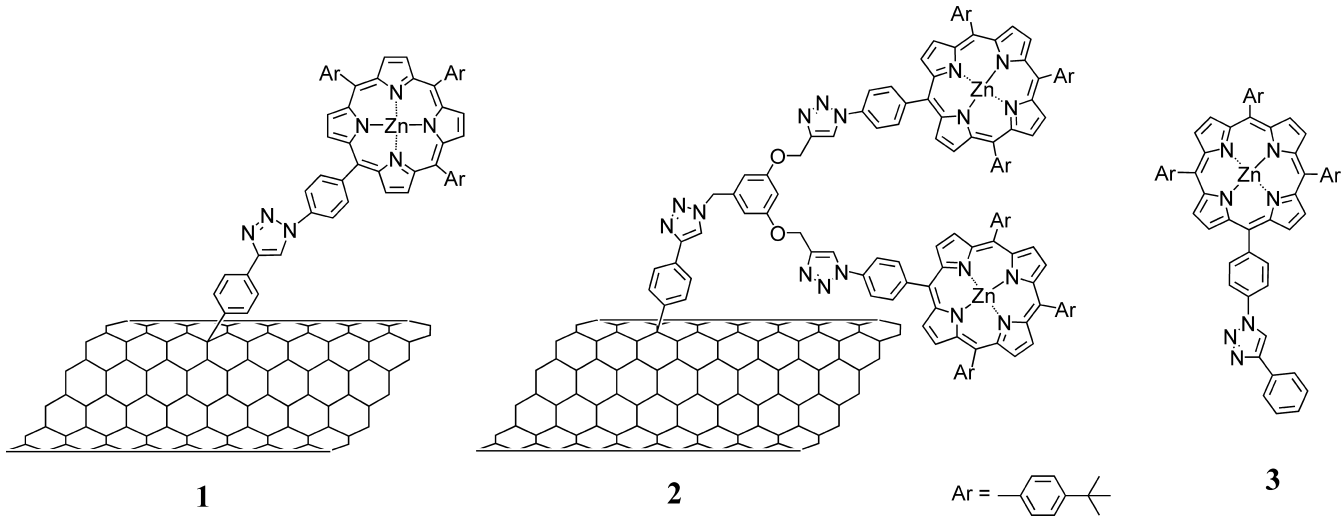

1 2 3

that combine the properties of SWNTs with those of the photoactive molecules.[1,27−31]

Among the different classes of electron donors that have been attached successfully to carbon nanotubes, porphyrinoid assemblies offer a myriad of incentives. Porphyrins possess exceptional optical and electronic properties. Their synthesis is simple and versatile. Moreover, the porphyrin core is outstandingly stable. The synthesis of a large series of SWNT−porphyrin electron donor−acceptor conjugates/hybrids has been reported either via covalent[2,32−37] or noncovalent means.[2,28,38−44]

In our group, we are particularly interested in the covalent functionalization of SWNTs with photoactive species. When compared to noncovalent methodologies, formation of SWNT conjugates employing covalent methods bears a number of advantages. First, the spacer that is used to link SWNT and the photoactive molecule is stable and well defined. Second, the number of functional groups is controlled by fine-tuning the functionalization processes. However, fabrication of the envisaged SWNT−ZnP electron donor−acceptor conjugates is still limited by the tremendous difficulties associated with incorporating sophisticated molecules onto the SWNT surfaces. There is a need for simple and versatile procedures that enable introducing new functionalities onto SWNTs. It is generally admitted that extensive covalent functionalization of SWNTs sidewalls disrupts the conjugated π-system of the tubes, affecting their optical and electronic properties;[45,46] this represents the main disadvantage of the covalent approach. However, limited functionalization processes might improve the processability of nanotubes while allowing the retention of their typical properties. In this context, functionalization of nanotubes with dendrimers represents a particularly promising strategy to attach a large number of functional groups onto the SWNT surfaces without significantly disturbing the conjugated π-system.[35]

The emerging field of "click chemistry" has the potential to provide an elegant protocol to prepare SWNT-based functional materials. In 2001, Sharpless introduced this approach into organic chemistry.[47] The term "click chemistry" defines a chemical reaction, which is versatile and clean and which requires simple workup and purification procedures. Among the many organic reactions, the Cu(I)-catalyzed variation of the *Huisgen* 1,3-dipolar cycloaddition[48] represents the most effective reaction in click chemistry. Recently, several examples of SWNT functionalization via click chemistry have been reported.[49−55] Our own contribution to this innovative field focused on the functionalization of SWNTs with phthalocyanines (Pc).[51] This work helped to establish that click chemistry permits incorporating photo- and electroactive building blocks on SWNTs. In fact, the resulting SWNT−ZnPc electron donor−acceptor conjugates were incorporated into photoelec-

(27) Sgobba, V.; Rahman, G. M. A.; Guldi, D. M.; Jux, N.; Campidelli, S.; Prato, M. *Adv. Mater.* **2006**, *18*, 2264.
(28) Chichak, K. S.; Star, A.; Altoé, M. V. P.; Stoddart, J. F. *Small* **2005**, *4*, 452.
(29) Hecht, D. S.; Ramirez, R. J. A.; Briman, M.; Artukovic, E.; Chichak, K. S.; Stoddart, J. F.; Grüner, G. *Nano Lett.* **2006**, *6*, 2031.
(30) Simmons, J. M.; In, I.; Campbell, V. E.; Mark, T. J.; Léonard, F.; Gopalan, P.; Eriksson, M. A. *Phys. Rev. Lett.* **2007**, *98*, 086802-1.
(31) Zhou, X.; Zifer, T.; Wong, B. M.; Krafcik, K. L.; Léonard, F.; Vance, A. L. *Nano Lett.* **2009**, *9*, 1028.
(32) Baskaran, D.; Mays, J. W.; Zhang, X. P.; Bratcher, M. S. *J. Am. Chem. Soc.* **2005**, *127*, 6916.
(33) Li, H.; Martin, R. B.; Harruff, B. A.; Carino, R. A.; Allard, L. F.; Sun, Y.-P. *Adv. Mater.* **2004**, *16*, 896.
(34) Guo, Z.; Du, F.; Ren, D.; Chen, Y.; Zheng, J.; Liu, Z.; Tian, J. *J. Mater. Chem.* **2006**, *16*, 3021.
(35) Campidelli, S.; Sooambar, C.; Lozano-Diz, E.; Ehli, C.; Guldi, D. M.; Prato, M. *J. Am. Chem. Soc.* **2006**, *128*, 12544.
(36) Cheng, F.; Adronov, A. *Chem. Mater.* **2006**, *18*, 5389.
(37) Liu, Z. B.; Tian, J.-G.; Guo, Z.; Ren, D.-M.; Du, F.; Zheng, J.-Y. *Adv. Mater.* **2008**, *20*, 511.
(38) Hasode, T.; Fukuzumi, S.; Kamat, P. V. *J. Am. Chem. Soc.* **2005**, *127*, 11884.
(39) Rahman, G. M. A.; Guldi, D. M.; Campidelli, S.; Prato, M. *J. Mater. Chem.* **2006**, *16*, 62.
(40) Ehli, C.; Rahman, G. M. A.; Jux, N.; Balbinot, D.; Guldi, D. M.; Paolucci, F.; Marcaccio, M.; Paolucci, D.; Melle-Franco, M.; Zerbetto, F.; Campidelli, S.; Prato, M. *J. Am. Chem. Soc.* **2006**, *128*, 11222.
(41) Cheng, F.; Adronov, A. *Chem.—Eur. J.* **2006**, *12*, 5053.
(42) Cheng, F.; Zhang, S.; Adronov, A.; Echegoyen, L.; Diederich, F. *Chem.—Eur. J.* **2006**, *12*, 6062.
(43) Chitta, R.; Sandanayaka, A. D.; Schumacher, A. L.; D'Souza, L.; Araki, Y.; Ito, O.; D'Souza, F. *J. Phys. Chem. C* **2007**, *111*, 6947.
(44) D'Souza, F.; Chitta, R.; Sandanayaka, A. S. D.; Subbaiyan, N. K.; D'Souza, L.; Araki, Y.; Ito, O. *Chem.—Eur. J.* **2007**, *13*, 8277.
(45) Cabana, J.; Martel, R. *J. Am. Chem. Soc.* **2007**, *129*, 2244.
(46) Cognet, L.; Tsyboulski, D. A.; Rocha, J.-D. R.; Doyle, C. D.; Tour, J. M.; Weisman, R. B. *Science* **2007**, *316*, 1465.
(47) Kolb, H. C.; Finn, M. G.; Sharpless, K. B. *Angew. Chem., Int. Ed.* **2001**, *40*, 2004.
(48) Huisgen, R. *Angew. Chem., Int. Ed. Engl.* **1968**, *7*, 321.
(49) Li, H.; Cheng, F.; Duft, A. M.; Adronov, A. *J. Am. Chem. Soc.* **2005**, *127*, 14518.
(50) Liu, J.; Nie, Z.; Gao, Y.; Adronov, A.; Li, H. *J. Polym. Sci., Part A: Polym. Chem.* **2008**, *46*, 7187.

trochemical cells, which revealed promising photon-to-energy conversion efficiencies.

Here, we report the synthesis, characterization, and properties of two SWNT conjugates bearing ZnP (Chart 1). SWNT−ZnP **1** is a simple electron donor−acceptor conjugate, in which one ZnP per functional group is attached to SWNT. On the other hand, in SWNT−ZnP **2**, a first-generation dendron bearing two ZnP was chosen, due to its larger absorption cross section, for attachment to SWNT. The syntheses of the dendrons and the corresponding **1** and **2** were based on click chemistry. We also report on the synthesis of **3**, which emerged as an important reference for the electrochemical and photophysical studies.

Results and Discussion

The synthetic pathways toward SWNT−ZnP conjugate **1** and of reference porphyrin **3**[56] are summarized in Scheme 1. *f*-SWNTs **5** were synthesized by following the protocol that has previously been reported.[51] Briefly, pristine SWNTs prepared by laser ablation were dispersed in 35% HNO_3 and then heated at 110 °C for 4 h. After filtration and extensive washing with water, the nanotubes were redispersed in NaOH (2 M), filtered, and washed with NaOH (1 M), HCl (1 M), and then with water. Finally, the buckypaper was dispersed in H_2O_2 (30%), heated at 100 °C for 1 h, and then filtered and extensively washed with water. Purified SWNTs **4** were functionalized by adding 4-(2-trimethylsilyl)ethynylbenzenediazonium generated *in situ* from 4-(2-trimethylsilyl)ethynylaniline[57] and isoamyl nitrite, which afforded **5**. The deprotected SWNTs **6** were produced prior to their use by reaction of **5** with NBu_4F. The azidoporphyrin derivative **7** was synthesized using a recent literature procedure.[56] Reaction of SWNTs **6** with porphyrin **3** in the presence of $Cu(MeCN)_4PF_6$, 2,6-lutidine, and tris-(hydroxypropyltriazolylmethyl)amine (THPTA) used as ligand for Cu(I)[58] gave SWNT−ZnP **1**. The reference porphyrin **3**[56] was synthesized by reacting **7** with phenylacetylene in the presence of $Cu(MeCN)_4PF_6$, 2,6-lutidine and THPTA.

The synthesis of the SWNT−ZnP conjugate **2** is described in Scheme 2. In particular, reacting 3,5-(dipropargyloxy)benzyl chloride **8**[59] and azidoporphyrin **7** in the presence of $Cu(MeCN)_4PF_6$, 2,6-lutidine and THPTA gave **9**. This benzyl chloride derivative was converted into **10** by reaction with sodium azide. Finally, compound **10** was allowed to react with the SWNTs **6** to give the SWNT−ZnP conjugate **2** bearing porphyrin dendrons of first generation.

SWNT−ZnP conjugates **1** and **2** were fully characterized by Raman, X-ray photoelectron (XPS), absorption and emission spectroscopy, atomic force microscopy (AFM), and electrochemistry. The Raman spectra of **1**, **2**, **3**, **4**, and **5** are shown in Figure 1. First of all, no noticeable effect of the functionalization was observed on the radial breathing mode (RBM, between 150−200 cm^{-1}) and tangential mode (G-band, between 1500−1650 cm^{-1}) features of SWNT, while we noticed a radical change in the relative intensity of the D-band after the first functionalization process, that is, the aryl diazonium addition. The increase of the D-band intensity is associated with the transformation of sp^2 carbons of the SWNT framework into sp^3 carbons. More important is that the intensity of this band remains constant after the click chemistry steps, indicating that the second reaction takes place on the triple bonds appended to the SWNT rather than directly on the SWNT sidewalls. Additional bands, attributed to ZnP, are also clearly discernible in the spectra of **1** and **2**. In fact, the new features appear to be more intense in **2**, an observation that is well in accordance with the composition of **1** and **2** featuring one and two ZnP, respectively.

XPS spectra recorded for **1**, **2**, **4**, and **5** give rise to the spectroscopic signature of carbon and oxygen for all the samples (Figure 2, left) and in some cases of nitrogen and zinc. Oxygen is present in the all samples, which is likely to originate from defects sites, alcohol or carboxylic acid functional groups, that were introduced during the purification process of SWNTs. An important observation is the lack of nitrogen in purified SWNTs **4**. In stark contrast, nitrogen is discernible in *f*-SWNTs **5** with a peak centered at 400.3 eV. It is, however, unlikely that the nitrogen is associated with the phenyl rings that have been

Scheme 1[a]

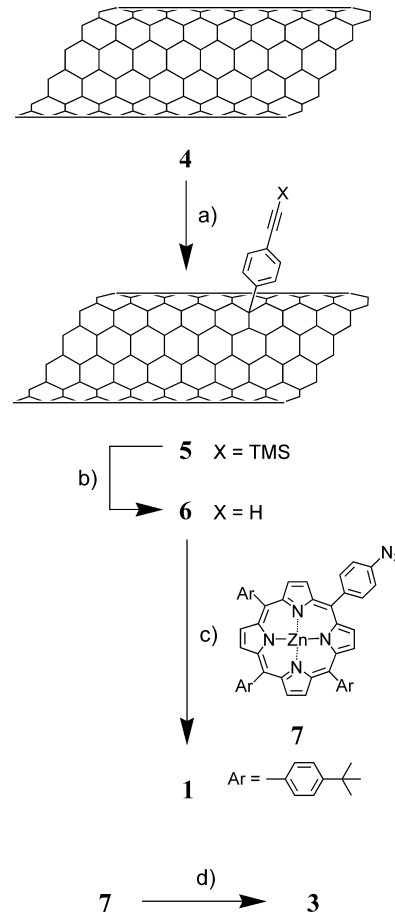

[a] Reagents and conditions: a) 4-(2-Trimethylsilyl)ethynylaniline, isoamyl nitrite, *N*-methylpyrrolidone (NMP), 80 °C; b) NBu_4F, NMP, rt; c) $Cu(MeCN)_4PF_6$, 2,6-lutidine, tris-(hydroxypropyltriazolylmethyl)amine (THPTA) NMP, rt; d) phenylacetylene, $Cu(MeCN)_4PF_6$, 2,6-lutidine, THPTA, THF/H_2O, 60 °C, 60%.

(51) Campidelli, S.; Ballesteros, B.; Filoramo, A.; Díaz-Díaz, D.; de la Torre, G.; Torres, T.; Rahman, G. M. A.; Ehli, C.; Kiessling, D.; Werner, F.; Sgobba, V.; Guldi, D. M.; Cioffi, C.; Prato, M.; Bourgoin, J.-P. *J. Am. Chem. Soc.* **2008**, *130*, 11503.
(52) Guo, Z.; Liang, L.; Liang, J.-J.; Ma, Y.-F.; Yang, X.-Y.; Ren, D.-M.; Chen, Y.-S.; Zheng, J.-Y. *J. Nanopart. Res.* **2008**, *10*, 1077.
(53) Zhang, Y.; He, H.; Gao, C. *Macromolecules* **2008**, *41*, 9581.
(54) He, H.; Zhang, Y.; Gao, C.; Wu, J. *Chem. Commun.* **2009**, 1655.
(55) Voggu, R.; Suguna, P.; Chandrasekaran, S.; Rao, C. N. R. *Chem. Phys. Lett.* **2007**, *443*, 118.
(56) Séverac, M.; Le Pleux, L.; Scarpaci, A.; Blart, E.; Odobel, F. *Tetrahedron Lett.* **2007**, *48*, 6518.
(57) Hwang, J.-J.; Tour, J. M. *Tetrahedron* **2002**, *58*, 10387.
(58) Liu, X.-M.; Takur, A.; Wang, D. *Biomacromolecules* **2007**, *8*, 2653.
(59) Wu, P.; Feldman, A. K.; Nugent, A. K.; Hawker, C. J.; Scheel, A.; Voit, B.; Pyun, J.; Fréchet, J. M. J.; Sharpless, K. B.; Fokin, V. V. *Angew. Chem., Int. Ed.* **2004**, *43*, 3928.

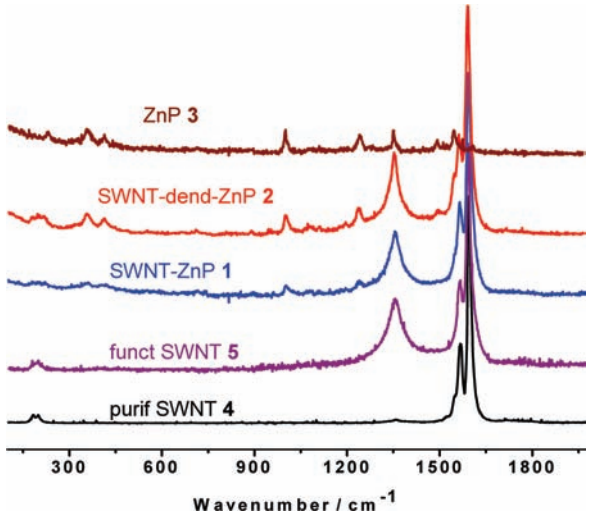

Figure 1. Raman spectra recorded after excitation at 457.9 nm of the purified SWNTs **4** (black), functionalized SWNTs **5** (purple), SWNT−ZnP **1** (blue), SWNT−dend-ZnP **2** (red) and ZnP **3** (brown). The intensities have been normalized (for SWNT derivatives) with respect to the high-frequency side of the G-band (ω_{G+}) at around 1590 cm^{-1}. The figure shows the evolution of the nanotubes during the functionalization processes: RBM (between 150−200 cm^{-1}) and G-band (between 1500−1650 cm^{-1}) are unaffected by the functionalization, while we observe a net increase of the D band at around 1300 cm^{-1} after the functionalization. New bands attributed to the porphyrin appear on the spectra of **1** and **2** after the click chemistry steps.

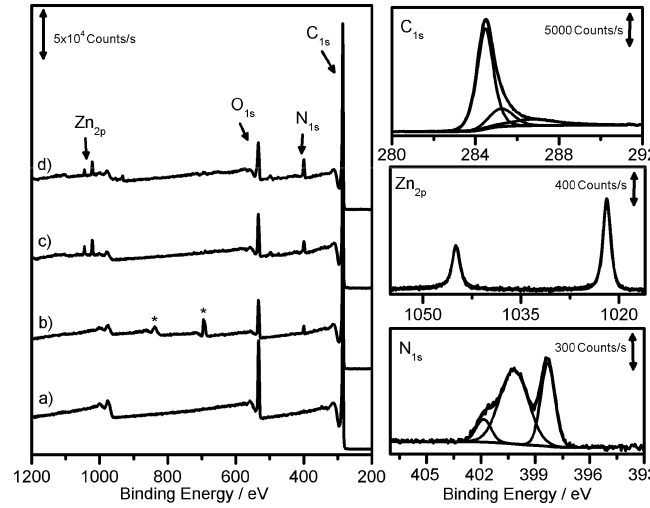

Figure 2. Left: XPS spectra of purified SWNTs **4** (a), functionalized SWNTs **5** (b), SWNT−ZnP **1** (c) and SWNT−dend-ZnP **2** (d) supported on PTFE membrane (asterisks in the spectrum show the fluorine from the membrane). Right: C 1s, Zn 2p, and N 1s core level spectra for SWNT−ZnP **1**.

grafted onto SWNTs. In fact, a reasonable explanation is the ability of SWNT to be spontaneously filled with fluids that have surface tensions below 100−200 mN/m.[60] Accordingly, the nitrogen signal may correspond to the solvent, namely *N*-methylpyrrolidone (NMP), which possesses a surface tension of 40.7 mN/m. This assumption was further corroborated by preparing buckypapers of pristine SWNT via sonication and filtration in either NMP or in water. In fact, only the XPS spectrum of the NMP-treated SWNT showed the typical nitrogen signal at 400.3 eV. The expanded N_{1s} regions of **1** (Figure 2, left) and **2** reveal three peaks. A single N_{1s} peak is observed at a binding energy of 398.3 eV, arising from the four nitrogen atoms of the metalloporphyrin macrocycle.[61] This peak proves the presence of ZnP in the nanotube derivatives **1** and **2**. Another N_{1s} peak located at 401.8 eV is attributed to one of the nitrogen atoms of the triazole ring,[62] while two remaining nitrogen atoms give rise to a peak at around 400.3 eV. The lack of a peak corresponding to free azide groups at 405 eV[63] unambiguously proves that azidoporphyrin **7** is covalently attached to the nanotube via a triazole ring and is not simply physisorbed on the surface by π-stacking interaction. Analysis of the Zn 2p region of **1** (Figure 2, left) and **2** shows two sharp peaks with binding energies at 1021.9 ($2p_{3/2}$) and 1044.9 eV ($2p_{1/2}$) in a 2:1 ratio due to Zn(II). A decomposition of C 1s energy level signal was performed for the SWNT−ZnP **1** and SWNT−dend-ZnP **2**. The peaks were deconvoluted with three Gaussian−Lorentzian curves at 284.4, 285.2, and 286.7 eV [see Figures 2 and S1 (Supporting Information (SI)]. Considering that the peak at 284.4 eV corresponds mainly to the electrons collected from the sp^2 carbons of CNTs, the calculation of the ratio of [Zn $2p_{3/2}$/C 1s] allows us to determine the number of functional groups on the nanotubes and the porphyrin ratio between **1** and **2**. For SWNT−ZnP **1**, we estimated a ratio of 1 functional group for 140 carbons (1 ZnP for 140 C), whereas it is only 1 functional group for 200 carbons in SWNT−dend-ZnP **2** (2 ZnP for 200 C). From this, one can conclude that there are 1.4 times more porphyrins in **2** than in **1**. This result shows that, as expected and as observed in the absorption spectra (Figure 5a), the amount of porphyrin is higher in **2** than in **1** but also that SWNT−dend-ZnP **2** is less functionalized than **1**.

The electrochemical properties of **1** and **2** were investigated by cyclic voltammetry. The nanotube derivatives were coated onto a platinum working electrode, and the electrochemical studies were performed at room temperature in acetonitrile containing tetrabutylammonium hexafluorophosphate (0.1 M). In Figure 3, the CVs of SWNT−ZnP **1** or SWNT−dend-ZnP **2**

Scheme 2[a]

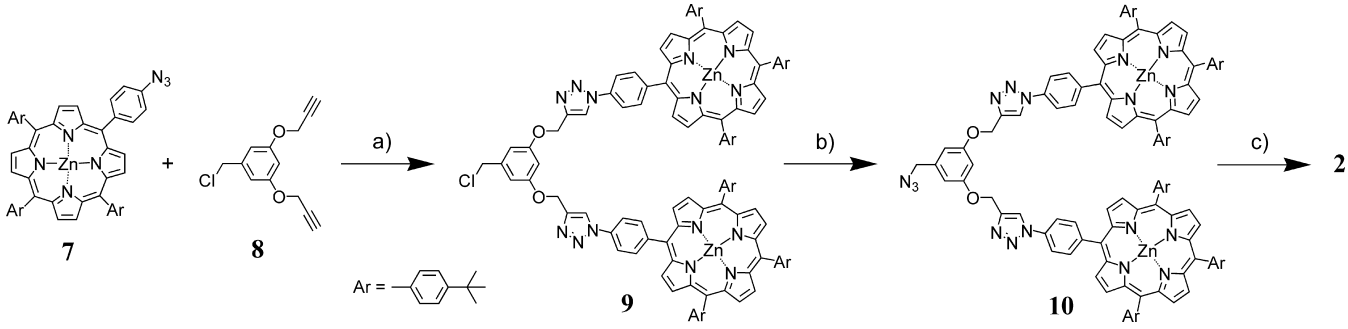

[a] Reagents and conditions: a) $Cu(MeCN)_4PF_6$, 2,6-lutidine, THPTA, THF/H_2O, 50 °C, 48%; b) NaN_3, THF/H_2O, 60 °C, 85%; c) SWNTs **6**, $Cu(MeCN)_4PF_6$, 2,6-lutidine, THPTA, NMP, rt.

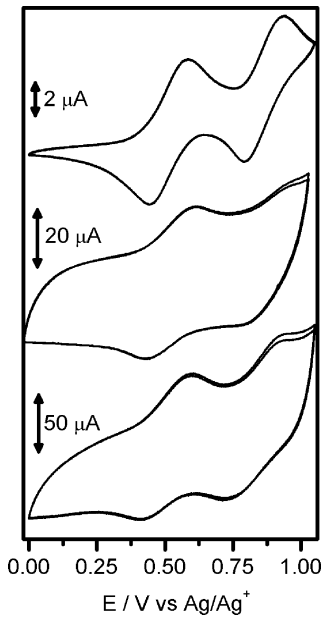

Figure 3. Cyclic voltammograms at 100 $mV \cdot s^{-1}$ of 1 mM ZnP **3** (top) solution (0.1 M Bu_4NPF_6/MeCN), of SWNT−ZnP **1** (middle) and SWNT−dend-ZnP **2** (bottom)-coated films in 0.1 M Bu_4NPF_6/MeCN, on platinum working electrode ($S = 0.07$ cm^2), potentials vs $Ag/AgNO_3$ (10^{-2} M).

show the porphyrin signature with the two reversible oxidation processes which are in perfect agreement with those of the reference porphyrin **3**. The high capacitive currents present in SWNT samples can be explained by the three-dimensional assembly of the working electrodes and the spaces between the nanotubes that can be filled by the electrolyte dissolved in acetonitrile.[64−66]

Next, **1**, **2**, and **5** were investigated by AFM. Three representative series of AFM images are shown in Figure 4. The topographic images reveal in all cases the presence of individual or very thin bundles of SWNTs. They are well dispersed on the surface with typical lengths that range from 500 nm to 2 μm. For **5**, the diameters were found to be around 1.5 nm, while slightly larger diameters were observed for SWNT−ZnP conjugates **1** and **2**, between 2 and 5 nm. The presence of ZnP might explain the difference in diameter distribution.

Absorption and emission spectra of the SWNT conjugates (**1**, **2**, and **5**) and that of the reference porphyrin (**3**) are shown in Figure 5. The absorption spectrum of **5** reflects a partial loss of the transitions between the van Hove singularities when compared to that of purified SWNT. This observation is in accordance with the generally observed modifications that arise from covalent attachment of organic moieties to the sidewalls of SWNT.[67] After the *Huisgen* cycloaddition, the spectra of SWNT−ZnP **1** and SWNT−ZnP **2** show three new maxima at

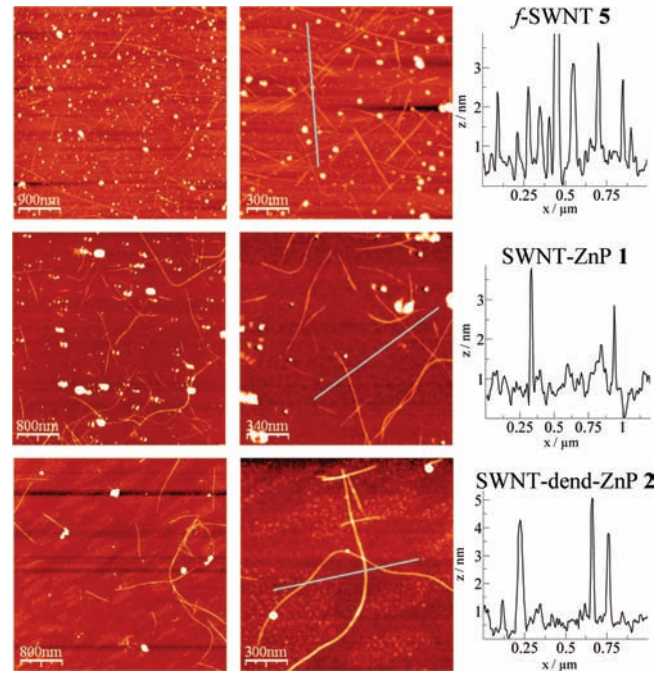

Figure 4. AFM images of *f*-SWNTs **5**, SWNT−ZnP **1**, and SWNT−dend-ZnP **2**. The images show the presence of small bundles and also individual nanotubes. The typical diameters of the different nanotube derivatives are shown on the right.

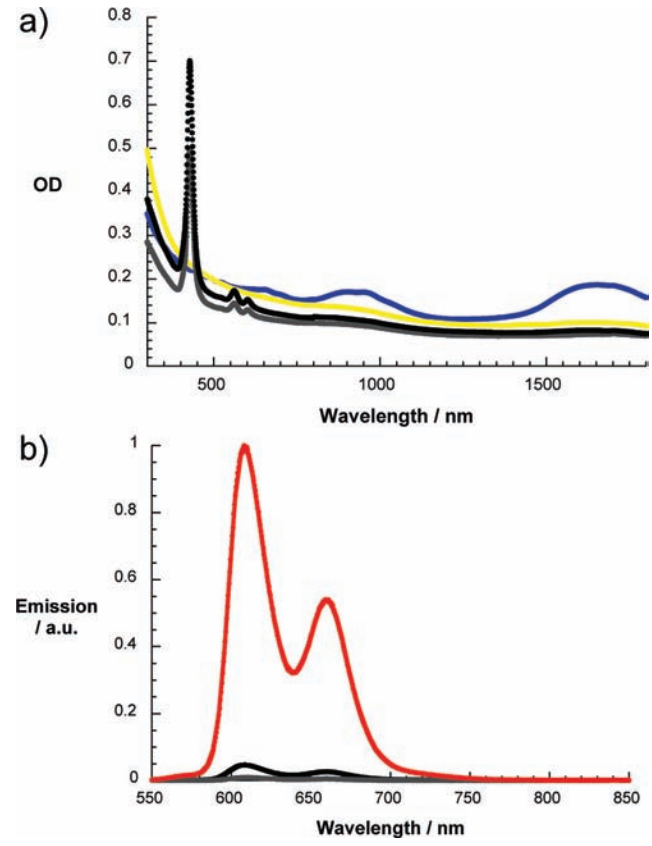

Figure 5. (a) Absorption spectra of purified SWNT (blue), *f*-SWNT **5** (yellow), SWNT−ZnP **1** (gray), and SWNT−ZnP **2** (black) in DMF. (b) Room temperature fluorescence spectra of SWNT−ZnP **1** (gray), SWNT−ZnP **2** (black), and ZnP **3** (red) in DMF with solutions that exhibit the same optical absorption at the 420 nm excitation wavelength.

427 and 561/601 nm, which correspond to the Soret- and the Q-bands of ZnP, respectively. In addition, the ratio of the ZnP

(60) Ebbesen, T. W. *J. Phys. Chem. Solids* **1996**, *57*, 951.
(61) Polzonetti, G.; Battocchio, C.; Goldoni, A.; Larciprete, R.; Carravetta, V.; Paolesse, R.; Russo, M. V. *Chem. Phys.* **2004**, *297*, 307.
(62) Ciampi, S.; Böcking, T.; Kilian, K. A.; James, M.; Harper, J. B.; Gooding, J. J. *Langmuir* **2007**, *23*, 9320.
(63) Collman, J. P.; Devaraj, N. K.; Eberspacher, T. P. A.; Chidsey, C. E. D. *Langmuir* **2006**, *22*, 2457.
(64) Marken, F.; Gerrard, M. L.; Mellor, I. M.; Mortimer, R. J.; Madden, C. E.; Fletcher, S.; Holt, K.; Foord, J. S.; Dahm, R. H.; Page, F. *Electrochem. Commun.* **2001**, *3*, 177.
(65) Rahman, M. M.; Jeon, I. C. *J. Braz. Chem. Soc.* **2007**, *18*, 1150.
(66) Krivenko, A. G.; Komarova, N. S. *Russ. Chem. Rev.* **2008**, *77*, 927.
(67) Dyke, C. A.; Tour, J. M. *J. Phys. Chem. A* **2004**, *108*, 11151.

centered features in **1** and **2** are approximately 1:2 (1 for 1.7 exactly) relative to the SWNT absorption. This trend is in perfect agreement with the structural features of **1** and **2** bearing one and two ZnP moieties, respectively. Insight into mutual interactions between SWNT and ZnP moieties came from fluorescence spectroscopy. Here, the high fluorescence quantum yield of ZnP, 0.04, is particularly helpful, since it allows monitoring energy- or charge-transfer processes with high precision even at relatively low concentrations. At first glance the ZnP fluorescence in **1** and **2** is strongly quenched, namely 99 and 96% for **1** and **2**, respectively (Figure 5). An independent confirmation for this assessment came from experiments where the optical absorption at the excitation wavelength was systematically varied over a broad range (Figure S2, SI). Correlating the corresponding slopes led to the same conclusion, namely, a nearly quantitative quenching of the ZnP fluorescence in **1** and **2**.

This led us to turn to transient absorption measurements following femtosecond excitation. Excitation of ZnP is accompanied by the rapid formation (i.e., 2 ps) of a transient that exhibits the following features: minima evolve at 425 and 560/600 nm, which correlate with the Soret- and Q-band absorptions of ZnP while maxima are seen at 455, 580, and 630 nm (Figure S3, SI). These features relate to the singlet−singlet absorptions of ZnP. Within the time window of 3.0 ns these singlet excited-state features transform (i.e., 2.4 ns) into those of the triplet excited state. The most prominent features of the latter are maxima at 475 and 840 nm (Figure S3, SI). The triplet excited state is long-lived with lifetimes of up to hundreds of microseconds in the absence of molecular oxygen.

The changes that were recorded upon excitation of either **1** or **2** are quite different, see Figures 6 and 7, for **1** and **2**, respectively. Following excitation at 387 nm we note two sets of features. The first set in the visible range corresponds to the singlet excited state of ZnP and attests to the successful excitation of ZnP (minima at 455, 580, and 630 nm). The second set in the near-infrared region is attributed to the SWNT centered excited states, which appear as mirror images of the ground-state absorption (see Figure 5 for comparison). In contrast to the differential absorption changes seen for ZnP, which give rise to a slow intersystem crossing, the ZnP singlet excited-state features decay rather rapidly in the presence of SWNT, namely 26 and 9 ps for **1** and **2**, respectively. For SWNT−ZnP **1** and **2**, at the conclusion of the fast decay, a newly developed band arising from 600 and 850 nm was observed. The close resemblance between this feature and what is known for the one-electron oxidized form of ZnP[68] leads us to conclude that charge transfers occur from ZnP singlet excited state to the nanotubes. It is important to notice that the 980 and 1605 nm minima of SWNT transform within the same time window into new features (i.e., minima at 940 and 1580 nm as well as a maximum at 1085 nm). An overall blue-shift of the SWNT centered transitions is observed, a feature that has been seen previously in spectroelectrochemical and pulse radiolytical reduction experiments[69] and which is linked to the injection of electrons into the conduction band of the semiconducting SWNT.

Quite similar kinetic decay and spectroscopic changes were observed for **1** and **2**. However, we observed that the radical

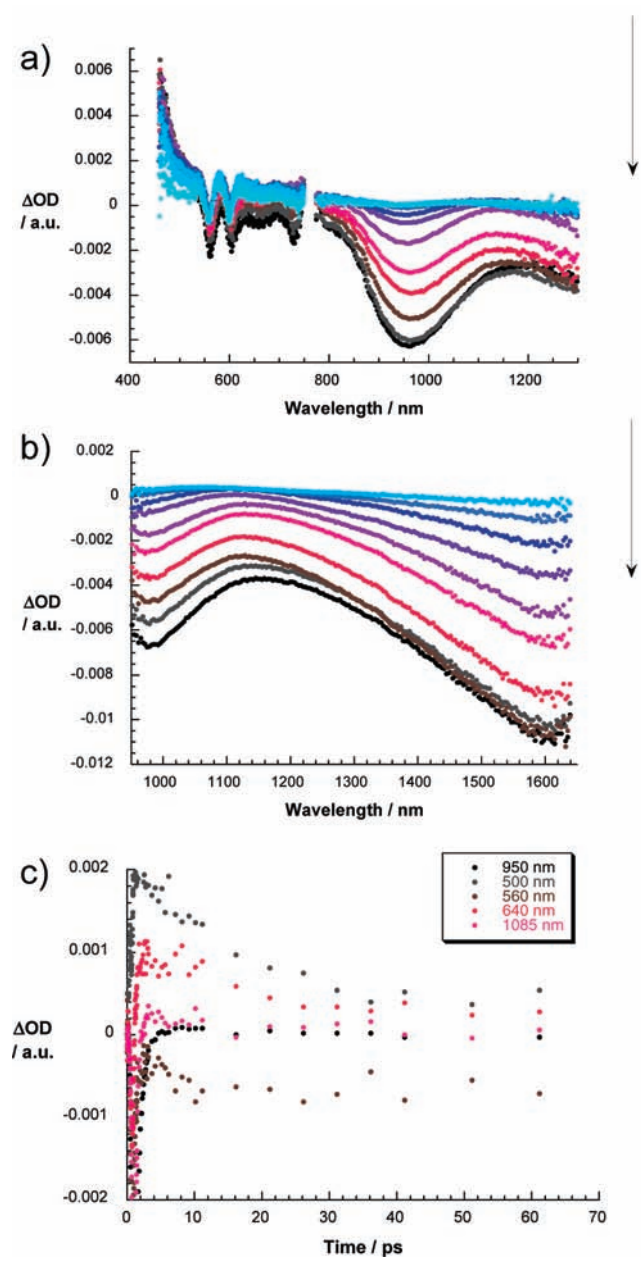

Figure 6. (a) Differential absorption spectra (visible and near-infrared range) obtained upon femtosecond flash photolysis (387 nm, 150 nJ) of SWNT−ZnP **1** in DMF with time delays between 1 ps (black) and 70 ps (blue) at room temperature. (b) Differential absorption spectra (extended near-infrared range) obtained upon femtosecond flash photolysis (387 nm, 150 nJ) of SWNT−ZnP **1** in DMF with time delays between 1 ps (black) and 70 ps (blue) at room temperature. (c) Time−absorption profiles of the spectra shown above at 500, 560, 640, 950, and 1085 nm, monitoring the charge transfer.

ion pair states were metastable in SWNT−ZnP **1** and **2**. The charge-separated states decay with lifetimes of 820 ps (**1**) and 200 ps (**2**) to regenerate the porphyrin singlet state. A likely rationale for the different charge-transfer kinetics implies the presence of the branching point (i.e., hydroxybenzyl moiety) in **2**. The latter induces structural flexibility in the molecule that allows ZnP to get close to the SWNT, increasing the electronic interactions between the two constituents. In fact, the

(68) Fukuzumi, S.; Imahori, H.; Yamada, H.; El-Khouly, M.; Fujitsuka, M.; Ito, O.; Guldi, D. M. *J. Am. Chem. Soc.* **2001**, *123*, 2571.

(69) Herranz, M. A.; Ehli, C.; Campidelli, S.; Gutiérrez, M.; Hug, G. L.; Ohkubo, K.; Fukuzumi, S.; Prato, M.; Martín, N.; Guldi, D. M. *J. Am. Chem. Soc.* **2008**, *130*, 66.

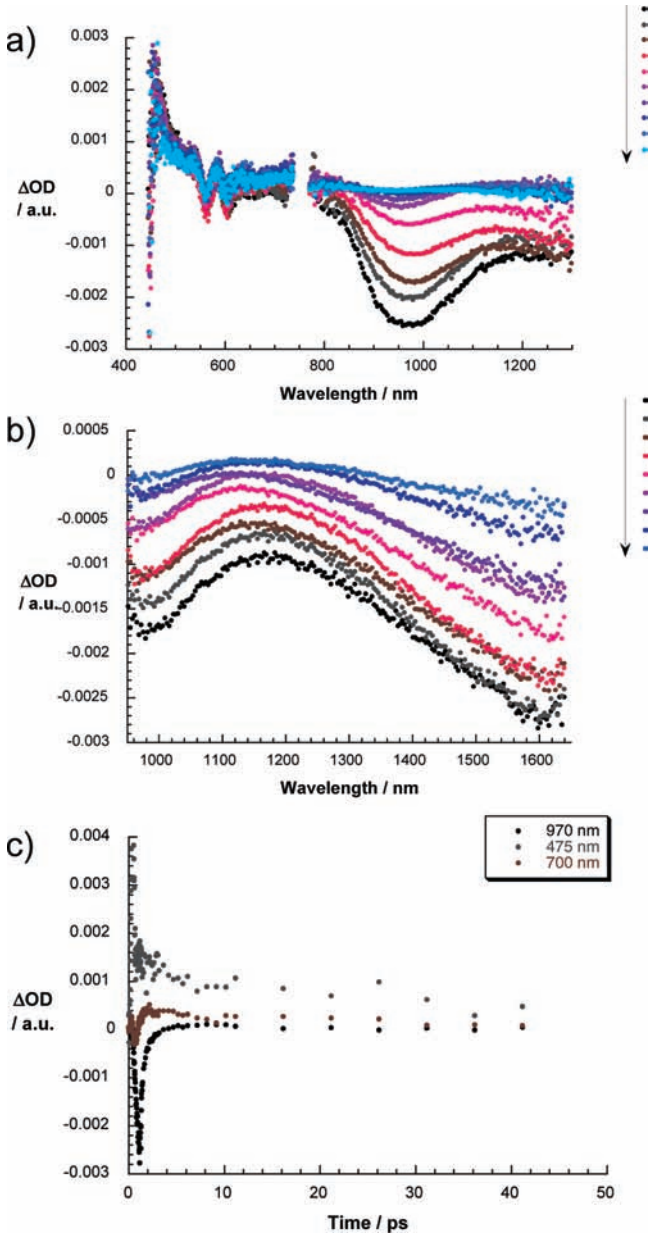

Figure 7. (a) Differential absorption spectra (visible and near-infrared range) obtained upon femtosecond flash photolysis (387 nm, 150 nJ) of SWNT−ZnP **2** in DMF with time delays between 1 ps (black) and 50 ps (blue) at room temperature. (b) Differential absorption spectra (extended near-infrared range) obtained upon femtosecond flash photolysis (387 nm, 150 nJ) of SWNT−ZnP **2** in DMF with time delays between 1 ps (black) and 50 ps (blue) at room temperature. (c) Time−absorption profiles of the spectra shown above at 475, 700, and 970 nm, monitoring the charge transfer.

SWNT/ZnP linker in **1** is conjugated and is therefore more rigid than the linker in SWNT−ZnP **2**. Molecular modeling further supports this assumption: in **1**, the distance between the porphyrin and the nanotube sidewall is estimated to ∼1.2 nm, while it is only 0.7 nm in the case of **2** (Figure S4, SI). Since these differences impact the communication between the two constituents, we postulate that in **1** and **2** charge transfer "through space" is more efficient than charge transfer "through bond".

Conclusion

In summary, we have described the novel synthesis of two SWNT−ZnP electron donor−acceptor conjugates (**1** and **2**). In **1**, one ZnP per functional group was introduced onto the SWNT surface, while the use of a first-generation dendron in **2** connects two ZnP to SWNT. This variation enabled fine-tuning the absorption cross section throughout the visible part of the solar spectrum. We have demonstrated that click chemistry is an efficient reaction for SWNT functionalization. In particular, it has permitted us to attach ZnP to SWNT using mild condition. Importantly, we succeeded in identifying the signature of the triazole ring by X-ray photoelectron spectroscopy, confirming unambiguously that the SWNT is linked covalently to ZnP. Photophysical assays by means of steady-state and time-resolved measurements reveal that the selective photoexcitation of ZnP in **1** and **2** is followed by a rapid charge separation, namely, the formation of reduced SWNT and oxidized ZnP. Due to the different spacers that link SWNT and ZnP, the radical ion pair states in **1** and **2** give rise to dissimilar lifetimes with values of 820 and 200 ps, respectively. The inherent flexibility of the dendritic part in SWNT−ZnP **2** favors a configuration, in which SWNT and ZnP are in close proximity to each other.

Experimental Section

Techniques. FTIR spectra were recorded on a Nicolet MAGMA-IR 860 spectrometer. ^{1}H NMR spectra were recorded with a BRUKER AC-300 (300 MHz) instrument with solvent used as internal reference. MALDI-TOF MS spectra were obtained from a Perseptive Biosystems Voyager DE-STR instrument. The Raman spectra were recorded using a Horiba Jobin-Yvon T64000 micro-raman system using an Ar-Kr laser as excitation source. For X-ray photoelectron spectroscopy (XPS) a Kratos Analytical Axis Ultra DLD, using an Al Kα source monochromatized at 1486.6 eV was used. We used a hemispheric analyzer working at pass energy of 50 eV for the global spectrum, and 20 eV when focusing on the sole core levels. All samples were supported on PTFE membrane. The electrochemical experiments were carried out using EG&G potentiostat, model 273A in a three-electrode electrochemical cell in atmospheric conditions. The experiments were conducted in anhydrous acetonitrile (water content <100 ppm) with tetrabutylammonium hexafluorophosphate $[Bu_4N]PF_6$ as the supporting electrolyte. The auxiliary electrode was a platinum wire. The reference electrode was based on the $Ag/AgNO_3$ 10^{-2} M couple. The working electrodes ($S = 0.07$ cm^2) were either a bare platinum electrode for the reference porphyrin **3** or a platinum electrode with a coated film of SWNT−ZnP **1** or SWNT−dend-ZnP **2**. Functionalized SWNTs were dispersed under ultrasounds in pure NMP and filtered on cellulose nitrate filters (Satorius, 0.45 μm), and then the membrane was deposited on a Pt electrode and dissolved through washings with acetone.[70] For the AFM analyses the samples were deposited on polylysine-coated silicon wafers from the NMP solution and incubated overnight; after washing with methanol and soft N_2 drying, the samples were investigated with a Veeco multimode scanning probe microscope equipped with a Nanoscope IIIa controller. Molecular modeling was performed using HyperChem software using MM+ method.

Photophysical Measurements. Steady-state absorption spectra were measured by a Cary5000 (Varian) two beam spectrometer. Emission spectra were recorded by using a FluoroMax-3 (HORIBA). The experiments were performed at room temperature. Femtosecond transient absorption studies were performed with 660 nm laser pulses (1 kHz, 150 fs pulse width, ∼100 nJ) from an amplified Ti:sapphire laser system (Clark-MXR, Inc.).

Materials. Laser ablation SWNTs were obtained from Dr. Oliver Jost (Dresden University). Chemicals were purchased from Aldrich and were used as received. Solvents were purchased from Aldrich

(70) Wu, Z.; Chen, Z.; Du, X.; Logan, J. M.; Sippel, J.; Nikolou, M.; Kamaras, K.; Reynolds, J. R.; Tanner, D. B.; Hebard, A. F.; Rinzler, A. G. *Science* **2004**, *305*, 1273.

or VWR and were used as received. For synthesis, CH_2Cl_2 (CaH_2, N_2), toluene (K/benzophenone, N_2), THF (K/benzophenone, N_2) were distilled before use. 5,10,15-Tris-(4-*tert*-butylphenyl)-20-(4-aminophenyl)porphyrin[56] and 3,5-(dipropargyloxy)benzyl chloride **8**[59] were synthesized according to the literature procedure.

Synthesis. Porphyrin 7. To a solution of zinc porphyrin **5** (100 mg, 0.116 mmol) in dry THF (40 mL) was added *tert*-butylnitrite (28 μL, 0.232 mmol) and azidotrimethylsilane (31 μL, 0.232 mmol) at 0 °C under Ar. The solution was stirred for 30 min and checked by TLC (eluent toluene). The completion of the reaction sometimes requires the addition of 2 additional equivalents of *tert*-butylnitrite and azidotrimethylsilane. Then water was added, and the mixture was extracted with CH_2Cl_2; the organic phase was filtered through hydrophobic paper filter (Phase Separator Whatman filter) and evaporated to dryness. Purification of the residue by column chromatography (eluent toluene) gave pure **6** (73 mg, 71% yield) as a pink powder. ^{1}H NMR (300 MHz, $CDCl_3$) δ 9.00 (d, 2H, arom H), 8.98 (s, 4H, arom H), 8.91 (d, 2H, arom H), 8.21 (d, 2H, arom H), 8.16 (d, 6H, arom H), 7.76 (d, 6H, arom H), 7.38 (d, 2H, arom H), 1.62 (s, 27H, $C(CH_3)_3$). FT-IR (KBr) υ (cm^{-1}) 2959, 2901, 2863, 2120, 2083, 1601, 1525, 1493, 1461, 1392, 1337, 1288, 1266, 1205, 1179, 1107, 1066, 998, 852, 800, 721, 694, 528. UV−vis (toluene) λ_{max} (nm) 425, 552, 592. MALDI-TOF MS $C_{56}H_{51}N_7Zn$ (885.35) m/z = 885.34 [M^+].

***p*-SWNTs 4.** Raw SWNT material (40 mg) was sonicated in nitric acid (35 vol %) (150 mL) with a sonic bath (160 W max) (100% for 5 min and then 40% for 15 min) and then heated at 100 °C for 4 h. The suspension was then cooled and vacuum filtered through a PTFE membrane (Sartorius, 0.2 μm pore). While pursuing vacuum filtration, the thick SWNT layer formed on the filtration membrane (buckypaper) was washed by 200 mL of deionized water; the pH was monitored during the washing and was about 7 at the end of the process. The nanotubes were redispersed in NaOH 2 M (100 mL) using the sonic bath (100% for 10 min) and then filtered through a PTFE membrane and washed with NaOH 2 M, deionized water, and then HCl 1 M followed by deionized water until the filtrate was neutral. Finally, the buckypaper was redispersed in hydrogen peroxide (30%) (150 mL) using the sonic bath (100% for 5 min and then 40% for 10 min). The suspension was heated at 100 °C for 1 h, cooled down to room temperature, and then vacuum filtered through a PTFE membrane. The nanotubes were washed by 200 mL of deionized water and then dried at 50 °C under high vacuum. The overall yield of the purification process was 45% (18 mg).

***f*-SWNTs 5.** A suspension of purified SWNTs **4** (15 mg) in NMP (50 mL) was first sonicated for 10 min and then 4-(2-trimethylsilyl)ethynylaniline[57] (475 mg, 2.5 mmol, 2 equiv C) and isoamyl nitrite (335 μL, 2.5 mmol, 22 equiv C) were added. The reaction mixture was stirred at 70 °C overnight under Ar. After cooling to room temperature, the suspension was filtered on a PTFE membrane (0.2 μm), and the black solid was washed several times with NMP. The nanotubes were redispersed in NMP (50 mL), and the entire procedure was repeated two times more. The SWNTs reacted in total with 6 equiv C of 4-(2-trimethylsilyl)ethynylaniline. A small part (less than 1.0 mg) of the solid on the filter was collected for analysis; the rest was redissolved and kept in NMP (90 mL; 1 mg SWNT per 6 mL of NMP).

SWNT−ZnP 1. To a suspension of *f*-SWNTs **5** (4 mg) in NMP (24 mL) at 0 °C was added a solution of tetrabutylammonium fluoride (1 M in THF) (10 μL). The reaction mixture was stirred at room temperature for 1 h, and then porphyrin **7** (10 mg, 11.0 μmol), $Cu(MeCN)_4PF_6$ (3 mg, 8.0 μmol), 2,6-lutidine (50 μL), and THPTA (a spatula tip) were added; then oxygen in the mixture was removed by several cycles of vacuum/argon. The reaction mixture was stirred at room temperature for 48 h and then filtered on a PTFE membrane (0.2 μm), washed with NMP, deionized water, saturated NH_4Cl solution, and then water and NMP. In order to remove the eventual products absorbed on the nanotubes, the buckypaper was redispersed in NMP, then refiltered and washed with NMP, THF, and CH_2Cl_2. These operations were repeated until the filtrate contained no porphyrin (checked by UV−vis absorption).

Porphyrin 3. To a solution of porphyrin **7** (15 mg, 0.017 mmol) in a mixture THF/water (10/1 mL) were added phenylacetylene (4 μL, 0.034 mmol), $Cu(MeCN)_4PF_6$ (3 mg, 0.008 mmol), 2,6-lutidine (100 μL), and THPTA (a spatula tip). The reaction mixture was frozen, and the oxygen was removed by several cycles of vacuum/argon. Finally, the solution was stirred at 60 °C for 20 h, then water was added, and the mixture was extracted with CH_2Cl_2; the organic phase was filtered through hydrophobic paper filter (Phase Separator Whatman filter) and evaporated to dryness. Purification of the residue by column chromatography (eluent CH_2Cl_2) gave pure **7** (10 mg, 60% yield) as a purple powder. ^{1}H NMR (300 MHz, $CDCl_3$) δ 8.04 (d, 2H, arom H), 9.00 (s, 4H, arom H), 8.95 (d, 2H, arom H), 8.53 (s, 1H, arom H), 8.43 (d, 2H, arom H), 8.21 (d, 2H, arom H), 8.16 (d, 6H, arom H), 8.05 (d, 2H, arom H), 7.77 (d, 2H, arom H), 7.55 (t, 2H, arom H), 7.48−7.40 (m, 1H, arom H), 1.63 (s, 27H, $C(CH_3)_3$). FT-IR (KBr) υ (cm^{-1}) 2958, 2901, 2865, 1525, 1492, 1461, 1394, 1362, 1338, 1267, 1205, 1109, 1070, 998, 853, 811, 796, 758, 719, 692, 582. UV−vis (toluene) λ_{max} (nm) 425, 550, 589. MALDI-TOF MS $C_{64}H_{57}N_7Zn$ (987.40) m/z = 987.42 [M^+].

Compound 9. To a solution of porphyrin **7** (50 mg, 0.056 mmol) in THF (10 mL) were added 3,5-(dipropargyloxy)benzyl chloride **8** (6.6 mg, 0.028 mmol), $Cu(MeCN)_4PF_6$ (5 mg, 0.014 mmol), 2,6-lutidine (100 μL), and water (1 mL). The reaction mixture was frozen, and the oxygen was removed by several cycles of vacuum/argon. Finally, the solution was stirred at 60 °C overnight, water was added, and the mixture was extracted with CH_2Cl_2; the organic phase was filtered through hydrophobic paper filter (Phase Separator Whatman filter) and evaporated to dryness. Purification of the residue by column chromatography (eluent first CH_2Cl_2, then CH_2Cl_2/Et_2O 100/5) gave pure **9** (27 mg, 48% yield) as a purple powder. Note that about 10 mg of monoadduct (compound containing only 1 porphyrin) was recovered from column chromatography. ^{1}H NMR (300 MHz, toluene-d_8, 60 °C) δ 9.15 (d, 4H, arom H), 9.11−9.06 (m, 8H, arom H), 8.94 (d, 4H, arom H), 8.31 (d, 4H, arom H), 8.26 (d, 8H, arom H), 8.05 (d, 4H, arom H), 7.05 (d, 4H, arom H), 6.79 (s, 2H, arom H), 6.57 (broad d, 2H, arom H), 6.25 (broad signal, 1H, arom H), 4.25 (s, 2H, CH_2Cl), 3.61 (broad s, 4H, OCH_2), 1.49 (s, 54H, $C(CH_3)_3$). FT-IR (KBr) υ (cm^{-1}) 2957, 2924, 2901, 2865, 1595, 1524, 1490, 1459, 1394, 1362, 1338, 1267, 1205, 1150, 1109, 1067, 1039, 998, 853, 811, 796, 719, 582. UV−vis (toluene) λ_{max} (nm) 424, 550, 590. MALDI-TOF MS $C_{125}H_{113}ClN_{14}O_2Zn_2$ (2004.74) m/z = 2004.68 [M^+].

Compound 10. To a solution of porphyrin **9** (20 mg, 0.010 mmol) in THF (5 mL) was added sodium azide (6.5 mg, 0.100 mmol) in water (1 mL). The reaction mixture was stirred under reflux for 1 day, and then water was added, and the mixture was extracted with CH_2Cl_2; the organic phase was filtered through hydrophobic paper filter (Phase Separator Whatman filter) and evaporated to dryness. Purification of the residue by column chromatography (eluent first CH_2Cl_2, then CH_2Cl_2/Et_2O 100/5) gave pure **10** (17 mg, 85% yield) as a purple powder. ^{1}H NMR (300 MHz, toluene-d_8, 60 °C) δ 9.14 (d, 4H, arom H), 9.10−9.05 (m, 8H, arom H), 8.93 (d, 4H, arom H), 8.30 (d, 4H, arom H), 8.25 (d, 8H, arom H), 8.06 (d, 4H, arom H), 7.15 (d, 4H, arom H), 6.91 (s, 2H, arom H), 6.44 (broad d, 2H, arom H), 6.35 (broad signal, 1H, arom H), 3.82 (broad signal, 6H, CH_2N and OCH_2), 3.61 (broad s, 4H, CH_2N), 1.49 (s, 54H, $C(CH_3)_3$). FT-IR (KBr) υ (cm^{-1}) 2954, 2924, 2901, 2864, 2095, 1594, 1523, 1490, 1458, 1393, 1362, 1338, 1266, 1204, 1150, 1108, 1066, 1039, 997, 852, 810, 796, 719, 581. UV−vis (toluene) λ_{max} (nm) 425, 552, 592. MALDI-TOF MS $C_{125}H_{113}N_{17}O_2Zn_2$ (2011.78) m/z = 2011.84 [M^+].

SWNT−ZnP 2. To a suspension of *f*-SWNTs **5** (3 mg) in NMP (18 mL) at 0 °C was added a solution of tetrabutylammonium fluoride (1 M in THF) (10 μL). The reaction mixture was stirred at room temperature for 1 h, and then porphyrin dendron **10** (10 mg, 5.0 μmol), $Cu(MeCN)_4PF_6$ (3 mg, 8.0 mmol), 2,6-lutidine (20 μL),

and THPTA (a spatula tip) were added; then oxygen in the mixture was removed by several cycles of vacuum/argon. The reaction mixture was stirred at room temperature for 72 h, filtered on a PTFE membrane (0.2 μm), and washed with NMP, deionized water, saturated NH_4Cl solution and then water and NMP. In order to remove the eventual products absorbed on the nanotubes, the buckypaper was redispersed in NMP, then refiltered and washed with NMP, THF, and CH_2Cl_2. These operations were repeated until the filtrate contained no porphyrin (checked by UV−vis absorption).

Acknowledgment. This work was carried out with the partial support from ANR (project Panini, ANR-07-ARFU-008), SFB 583, DFG (GU 517/4-2), FCI and the Office of Basic Energy Sciences of the U.S. Department of Energy. We thank Dr. Oliver Jost (Dresden University) for providing the SWNTs.

Supporting Information Available: Additional characterization for porphyrin and nanotube-porphyrin derivatives. This material is available free of charge via the Internet at http://pubs.acs.org.

JA906020E